Report

Cell Reports

Adaptive Resistance to an Inhibitor of Chromosomal Instability in Human Cancer Cells

Graphical Abstract

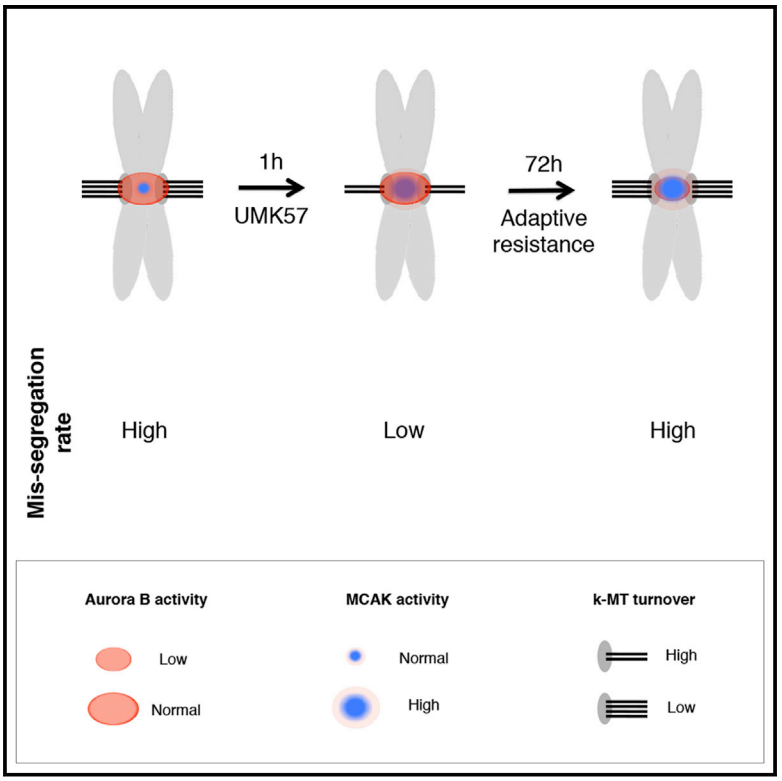

Authors

Bernardo Orr, Lama Talje, Zhexian Liu, Benjamin H. Kwok, Duane A. Compton

Correspondence

benjamin.kwok@umontreal.ca (B.H.K.), duane.a.compton@dartmouth.edu (D.A.C.)

In Brief

Orr et al. describe a compound that transiently suppresses mis-segregation in CIN cells. This is accompanied by alterations in mitotic signaling pathways that are consistent with adaptive resistance. These results shed light on drug resistance in CIN cells and highlight the underappreciated role of CIN in cancer relapse.

Highlights

- UMK57 potentiates MCAK in vivo
- UMK57 transiently suppresses chromosome mis-segregation in CIN cancer cells
- CIN cancer cells display adaptive resistance to UMK57
- Rate of adaptive resistance in UMK57-treated cells is Aurora B-dependent

Orr et al., 2016, Cell Reports *17*, 1755–1763
November 8, 2016
http://dx.doi.org/10.1016/j.celrep.2016.10.030

Cell Reports
Report

Adaptive Resistance to an Inhibitor of Chromosomal Instability in Human Cancer Cells

Bernardo Orr,[1,2] Lama Talje,[3] Zhexian Liu,[3] Benjamin H. Kwok,[3,4,*] and Duane A. Compton[1,2,5,*]
[1]Department of Biochemistry and Cell Biology, Geisel School of Medicine at Dartmouth, Hanover, NH 03755, USA
[2]Norris Cotton Cancer Center, Lebanon, NH 03766, USA
[3]Institute for Research in Immunology and Cancer, Université de Montréal, Québec H3T 1J4, Canada
[4]Département de Médecine, Université de Montréal, Québec H3T 1J4, Canada
[5]Lead Contact
*Correspondence: benjamin.kwok@umontreal.ca (B.H.K.), duane.a.compton@dartmouth.edu (D.A.C.)
http://dx.doi.org/10.1016/j.celrep.2016.10.030

SUMMARY

Karyotype diversity is a hallmark of solid tumors that contributes to intratumor heterogeneity. This diversity is generated by persistent chromosome mis-segregation associated with chromosomal instability (CIN). CIN correlates with tumor relapse and is thought to promote drug resistance by creating a vast genomic landscape through which karyotypically unique clones survive lethal drug selection. We explore this proposition using a small molecule (UMK57) that suppresses chromosome mis-segregation in CIN cancer cells by potentiating the activity of the kinesin-13 protein MCAK. Sublethal doses of UMK57 destabilize kinetochore-microtubule (k-MT) attachments during mitosis to increase chromosome segregation fidelity. Surprisingly, chromosome mis-segregation rebounds in UMK57-treated cancer cells within a few days. This rapid relapse is driven by alterations in the Aurora B signaling pathway that hyper-stabilize k-MT attachments and is reversible following UMK57 removal. Thus, cancer cells display adaptive resistance to therapies targeting CIN through rapid and reversible changes to mitotic signaling networks.

INTRODUCTION

Aneuploidy is a hallmark of solid tumors (Luo et al., 2009) and commonly arises in tumors through the frequent mis-segregation of whole chromosomes as a consequence of chromosomal instability (CIN) (Geigl et al., 2008; Lengauer et al., 1997). Persistent chromosome mis-segregation is a major driver of intra-tumor heterogeneity (Heppner, 1984), a genomic change that is proposed to allow cells to acquire new phenotypes (Duesberg et al., 2000; Gerlinger and Swanton, 2010). Accordingly, CIN positively correlates with poor patient prognosis (Bakhoum et al., 2011), multidrug resistance (Lee et al., 2011), and tumor relapse (Sotillo et al., 2010). The prevailing model posits that CIN generates a genomic landscape from which clones and sub-clones with specific karyotypes emerge from the population through survival of targeted therapy and/or other selective pressures (Greaves and Maley, 2012). Directly testing this model requires the development of tools that specifically suppress CIN in human cancer cells.

The root cause of CIN is the persistence of errors in kinetochore-microtubule (k-MT) attachments in mitosis (Thompson and Compton, 2008). Errors in k-MT attachment arise spontaneously during mitosis and are efficiently corrected in diploid cells to preserve genome integrity. The correction process relies on the frequent detachment of microtubules from kinetochores to allow for microtubules with the proper orientation to make attachments. It was previously demonstrated that many CIN cancer cells have hyper-stable k-MT attachments and fail to efficiently correct k-MT attachment errors (Bakhoum et al., 2009a). Importantly, strategically destabilizing k-MT attachments by overexpressing the microtubule-destabilizing kinesin-13 proteins Kif2b and MCAK suppresses CIN in cancer cells and establishes a causative relationship between the stability of k-MT attachments and the rate of chromosome mis-segregation (Bakhoum et al., 2009a, 2009b, 2014; Kleyman et al., 2014). These data provide proof of concept for a strategy to suppress CIN in human cancer cells. Unfortunately, this strategy is severely limited by the requirement for protein overexpression in tumor cells. To overcome this technical limitation and to examine how cancer cells respond to the suppression of CIN, we examine the effects of a cell-permeable small molecule that potentiates the microtubule depolymerizing activity of the kinesin-13 protein MCAK.

RESULTS AND DISCUSSION

UMK57 Potentiates MCAK Activity

Current strategies for the suppression CIN in cancer cells rely on the manipulation of proteins involved in the regulation of k-MT attachments during mitosis (Bakhoum et al., 2009b; Ertych et al., 2014), which prove to be limiting outside of cell culture. To overcome these limitations, a high-throughput screen was performed to identify small molecules that modulate the activities of kinesin-13 proteins (Talje et al., 2014). This screen identified a kinesin-13 inhibitor that was previously reported (Talje et al., 2014). This screen also identified a family of compounds that potentiate the microtubule depolymerizing activity

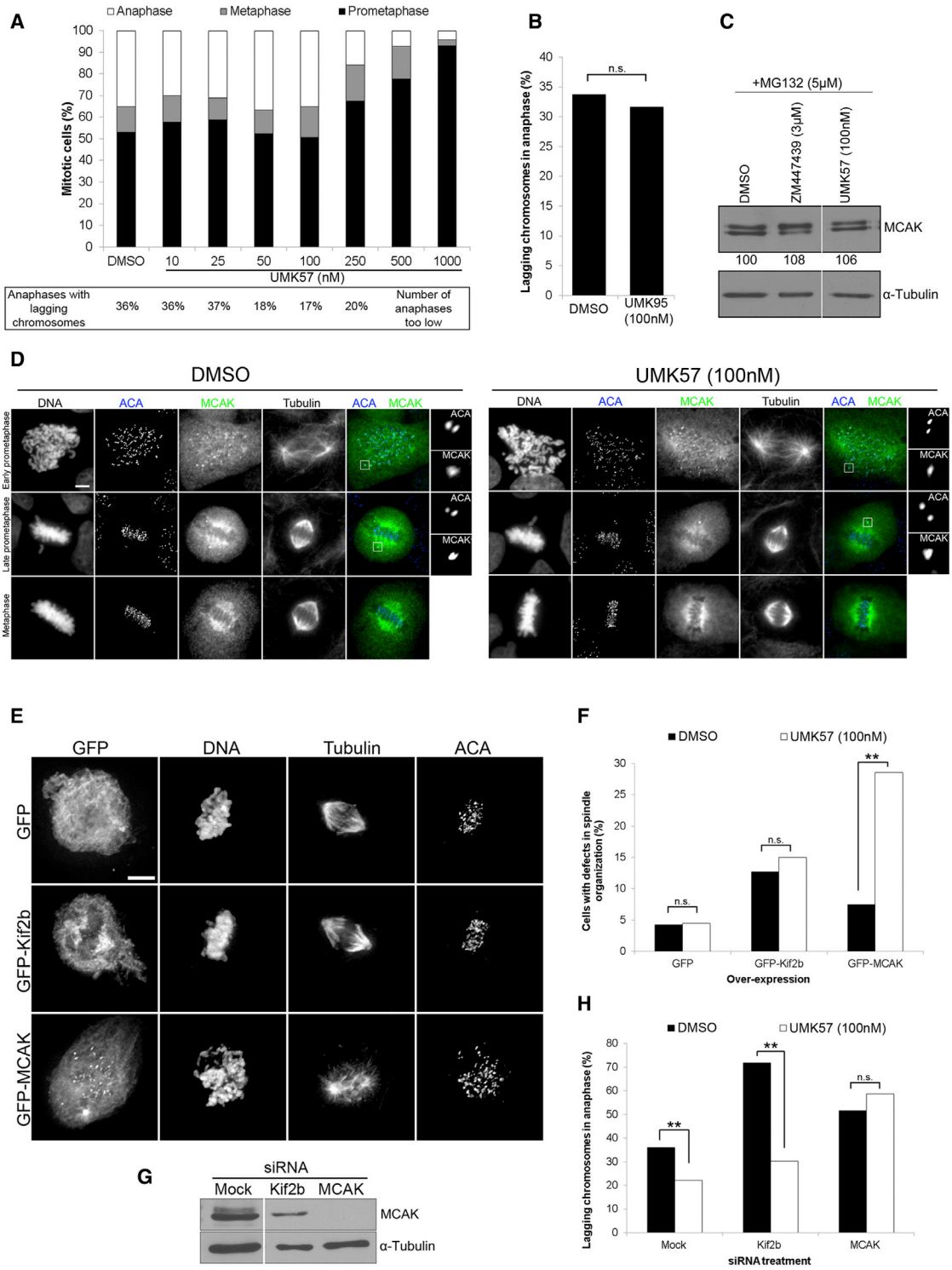

Figure 1. UMK57 Targets MCAK In Vivo but Does Not Alter Its Levels or Localization in Cells

(A) Percentage of mitotic cells in prometaphase, metaphase, or anaphase in cells treated with DMSO or increasing concentrations of UMK57 for <1 hr ($n \geq 200$ mitotic cells). For each concentration of UMK57, the percentage of anaphases with lagging chromosomes is shown below ($n \geq 150$ anaphases).

(B) Lagging chromosome rates of U2OS cells treated with DMSO or UMK95, a chemical probe that is structurally similar to UMK57 but inactive in vitro ($n \geq 150$ anaphases); n.s., $p > 0.05$ using Fisher's exact two-tailed test.

(legend continued on next page)

of kinesin-13 proteins in vitro, and the complete characterization of how these compounds affect the biochemistry of kinesin-13 proteins in vitro will be provided elsewhere. Here, we focus on the effects of one of these compounds (UMK57) on chromosome segregation during mitosis in vivo. We focused on UMK57 because it shows no inhibitory effect on the ATPase activity of any kinesins tested (Figure S1A) but specifically enhances MCAK-dependent microtubule depolymerization as measured using in vitro microtubule sedimentation (Figure S1B) and microscopy (Figure S1C) assays. Additionally, UMK57 inhibits cell proliferation in a dose-dependent manner (Figure S1D). In contrast, a chemically related analog differing only in one chemical group (UMK95) has no effect on MCAK-mediated microtubule depolymerization (Figure S1B) or cell proliferation (Figure S1D), demonstrating the potency and specificity of UMK57 (Figures S1E and S1F).

Titration experiments in U2OS cells demonstrate that 100 nM UMK57 is the optimal dose to achieve the maximal effect on the fidelity of chromosome segregation without significantly affecting mitotic progression (Figure 1A); therefore, all treatments were done at this concentration, unless stated otherwise. Treatment of cells with UMK95, a chemically related but inactive compound (Figure S1F), shows no detectable effect on chromosome segregation (Figure 1B), underscoring the specificity of UMK57 (Arrowsmith et al., 2015) (Figure S1E). It is important to note that treatment of cells with 100 nM UMK57 does not alter total MCAK levels (Figure 1C), MCAK localization, or spindle organization at different stages of mitosis (Figures 1D). Also, very few UMK57-treated cells transiently expressing GFP or GFP-Kif2b show discernible defects in chromosome alignment or spindle bipolarity (Figures 1E and 1F). In contrast, a substantial fraction of UMK57-treated cells transiently expressing GFP-MCAK display defects in chromosome alignment and spindle organization, indicating that MCAK overexpression renders cells hypersensitive to UMK57 (Figures 1E and 1F). In addition, UMK57 reduces the rate of chromosome mis-segregation in control and Kif2b-depleted cells (Figures 1G and 1H). However, there is no change in the rate of chromosome mis-segregation in MCAK-depleted cells (Figures 1G and 1H). This indicates that the effects of UMK57 in mitosis are dependent on the presence of MCAK.

UMK57 Suppresses CIN in Human Cancer Cells

To determine the effect of UMK57 on chromosome segregation in different human cell lines, we quantified lagging chromosome rates in anaphase in CIN cancer lines (U2OS, HeLa, and SW-620) and in non-transformed diploid cell lines (hTERT-immortalized RPE-1 and BJ). Treatment with UMK57 significantly reduces lagging chromosome rates in all cancer cell lines tested but has no effect on chromosome segregation in the non-transformed diploid cell lines (Figures 2A and 2B). Given that many lagging chromosomes in anaphase can segregate to the correct daughter cell (Thompson and Compton, 2011), we tested whether UMK57 treatment also reduces the rate of chromosome non-disjunction. We measured the fate of sister chromatids of a single chromosome in HCT116 cells recovering from a monastrol-induced mitotic arrest using previously described methods (Lampson and Kapoor, 2005; Thompson and Compton, 2008, 2011). Cells treated with UMK57 display a significantly lower rate of chromosome non-disjunction than control cells (Figures 2C and 2D).

Next, we quantified the stability of k-MT attachments in UMK57-treated U2OS cells by measuring the rate of dissipation of fluorescence after photoactivation of GFP-tubulin (Zhai et al., 1995). The stability of k-MT attachments during metaphase in mitotic cells treated with UMK57 is reduced by more than 35% when compared to control cells, consistent with the potentiation of the microtubule depolymerase activity of MCAK (Figures 2E and S2A–S2C). There is no significant change in the stability of k-MT attachments in prometaphase, which is in agreement with previous reports indicating that MCAK preferentially destabilizes metaphase k-MTs in this cell line (Bakhoum et al., 2009b). Moreover, there are no significant differences in the fractions of microtubules in the stable (k-MT) versus unstable (non-k-MT) populations (Figure S2D) or in the turnover rate of the unstable population in UMK57-treated cells (Figure S2E). Despite the destabilization of k-MTs during metaphase, UMK57 treatment at this dose does not significantly alter mitotic progression (Figure 1A) but induces a subtle yet significant reduction in the interkinetochore distance of aligned kinetochore pairs (Figure 2F). However, UMK57 treatment does not affect chromosome bi-orientation or the spindle assembly checkpoint as judged by the localization patterns of Aurora B kinase (Figure S2F) or astrin (Figure S2G) and the levels of the mitotic checkpoint protein BubR1 at kinetochores (Figures 2G and 2H). Furthermore, RPE-1 and U2OS cell lines display differential sensitivity to UMK57, but not vinblastine, indicating that the effects of UMK57 are distinct from a compound that directly targets tubulin (Figures S2H–S2K). Collectively, these results demonstrate that UMK57 acts through an MCAK-dependent process to specifically destabilize k-MT attachments during metaphase and reduces chromosome mis-segregation with little or no appreciable effects on other mitotic processes. Thus, UMK57 is a small molecule that specifically promotes the correction of k-MT attachment errors to

(C) Quantitative western blot of mitotic U2OS cell extracts treated with MG132 for 4 hr to enrich the mitotic population and prevent mitotic exit and then treated with DMSO, ZM447439, or UMK57 for 1 hr and blotted for total MCAK and α-tubulin. Numbers below indicate the relative quantities (percentage) for each protein.
(D) U2OS cells treated with DMSO or UMK57 for <1 hr and then fixed and stained to reveal DNA, anti-centromere antibody (ACA; blue), MCAK (green), or α-tubulin. Insets represent 5× magnifications of selected regions (further contrasted for better visualization). Scale bar, 5 μm.
(E) U2OS cells transiently overexpressing GFP, GFP-Kif2b, or GFP-MCAK were treated with UMK57 (100 nM) and then fixed and stained to reveal DNA, α-tubulin, and ACA. Scale bar, 5 μm.
(F) Percentage of prometaphase cells with defects in spindle organization in cells overexpressing GFP, GFP-Kif2b, or GFP-MCAK and treated with DMSO or UMK57 (n > 150 prometaphase cells).
(G) Total cell lysates of Mock-, Kif2b-, and MCAK-depleted U2OS cells were immunoblotted for MCAK and α-tubulin (loading control).
(H) Quantification of lagging chromosome rates in Mock-, Kif2b-, or MCAK-depleted cells incubated with DMSO or UMK57 for <1 hr (n > 100 anaphases). All error bars represent SEM. **$p \leq 0.01$; n.s., $p > 0.05$ using Fisher's exact two-tailed test.

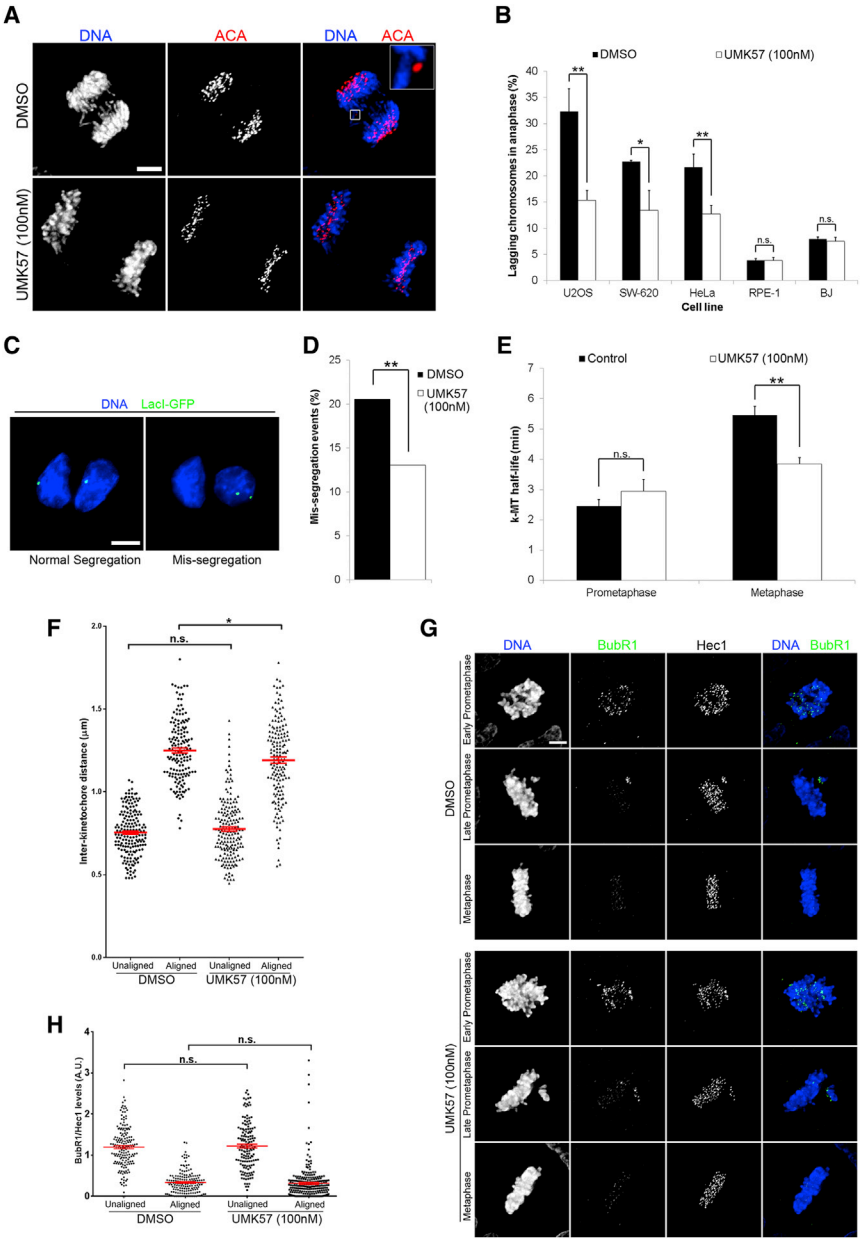

Figure 2. UMK57 Reduces Lagging Chromosome Rates in Human Cancer Cell Lines by Destabilizing k-MT Attachments in Metaphase

(A) Representative immunofluorescence image of U2OS cells in anaphase treated with DMSO or UMK57 for <1 hr and then fixed and stained to reveal DNA (blue) and ACA (red). Inset represents 5× magnification of selected region (further contrasted for better visualization). Scale bar, 5μm.

(B) Percentage of lagging chromosomes in anaphase in multiple cell lines after treatment with DMSO or UMK57 for <1 hr (n > 300 anaphases). Error bars represent SD from three independent experiments. *p ≤ 0.05; **p ≤ 0.01; n.s., p > 0.05 using Fisher's exact two-tailed test.

(C) Representative immunofluorescence image of segregation phenotypes in HCT116 cells expressing LacI-GFP with LacO arrays integrated into a single chromosome that were fixed and imaged after completion of cytokinesis. Scale bar, 5 μm.

(D) Quantification of total mis-segregation events in HCT116 cells expressing LacI-GFP with LacO arrays integrated into a single chromosome subjected to a monastrol washout into media containing DMSO or UMK57 and allowed to complete mitosis and re-enter interphase. Total mis-segregation was quantified as depicted in panel (C) (n > 600 pairs of daughter nuclei). **p ≤ 0.01 using Fisher's exact two-tailed test.

(E) Calculated k-MT half-life in U2OS cells treated with 5 μM MG132 (control) or 5 μM MG132 + UMK57 (100 nM); n = 12–19 cells. Graph shows mean ± SEM; **p ≤ 0.01; n.s., p > 0.05 using two-tailed t test.

(F) Quantification of inter-kinetochore distance as measured by distance between Hec1 staining in sister kinetochores in cells treated with DMSO or UMK57. Red bars indicate the mean and red error bars the SEM; n ≥ 150 kinetochores; *p ≤ 0.05; n.s., p > 0.05 using two-tailed t test.

(G) Cells treated with DMSO or UMK57 for <1 hr and then fixed and stained to reveal DNA (blue), BubR1 (green), and Hec1. Insets represent 5× magnifications of selected regions (further contrasted for better visualization). Scale bar, 5 μm.

(H) Quantification of BubR1 levels at kinetochores (normalized to Hec1) in U2OS cells treated with UMK57 (100 nM) for <1 hr as quantified by immunofluorescence. n ≥ 150 kinetochores from 10–20 cells; n.s., p > 0.05 using two-tailed t test. All error bars represent SEM.

suppress chromosome mis-segregation in CIN cancer cells, with no detectable effects on non-transformed diploid cells.

Resistance to UMK57 Treatment Arises Rapidly

The gold standard for assaying CIN is through the measurement of karyotypic diversity in colonies derived from single cells where chromosomally stable cells generate karyotypically homogeneous populations and CIN cells generate karyotypically heterogeneous populations (Bakhoum et al., 2009b; Lengauer et al., 1997; Thompson and Compton, 2008). To determine if UMK57 suppresses CIN in this context, we used fluorescence in situ hybridization (FISH) to determine the modal chromosome number for two different chromosomes and scored the percentage of cells that deviate from that mode in two independent colonies grown from single cells for each condition. Non-transformed RPE-1 cells maintain stable diploid karyotypes, and the fraction of cells that deviate from the modal chromosome copy number within each colony is very low and insensitive to UMK57 treatment (Figures 3A and 3B). U2OS cells are CIN, and the fraction of cells that deviate from the modal chromosome copy number within each colony is high. Surprisingly, treatment of U2OS cells with UMK57 continuously during colony growth (6–8 weeks) did

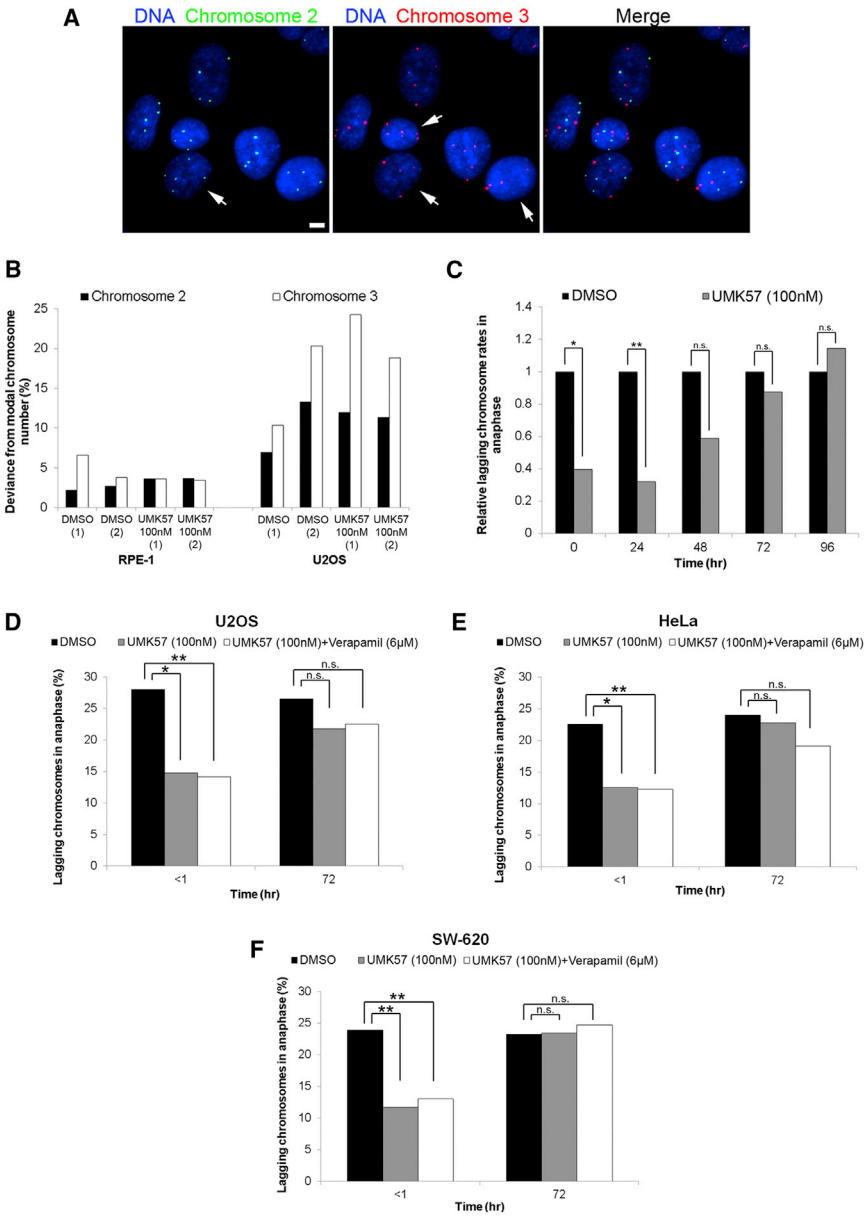

Figure 3. Long-Term Exposure to UMK57 Results in Decreased Responsiveness to UMK57-Mediated Suppression of CIN

(A) Example of FISH data from U2OS single-cell clones fixed and stained with DNA (blue) to visualize nuclei and with probes specific for centromeric α-satellite DNA of chromosomes 2 (green) and 3 (red). White arrows indicate cells whose chromosome copy number deviates from the modal chromosome number (Chr. 2, mode of 4; Chr. 3, mode of 5). Scale bar, 5 μm.

(B) Percentage of nuclei that deviate from the modal chromosome number in RPE-1 or U2OS single-cell clones grown in the presence of DMSO or UMK57. Chromosome copy number quantified for chromosomes 2 and 3 (n > 300 nuclei).

(C) Media with DMSO or UMK57 was prepared and added to U2OS cells at time 0. Cells were fixed and stained every 24 hr and lagging chromosome rates quantified every 24 hr. *$p \leq 0.05$; **$p \leq 0.01$; n.s., $p > 0.05$ using Fisher's exact two-tailed test. Media with DMSO, UMK57, or UMK57 + verapamil (MDR1 inhibitor) was prepared and added to cells at time 0.

(D–F) Cells were fixed and stained at <1 hr and 72 hr and lagging chromosome rates quantified for (D) U2OS cells (n > 300), (E) HeLa cells (n > 300), and (F) SW-620 cells (n > 200). Total lagging chromosome rates were pooled from two independent experiments; *$p \leq 0.05$; **$p \leq 0.01$; n.s., $p > 0.05$ using Fisher's exact two-tailed test. All error bars represent SEM.

not reduce the fraction of cells that deviate from the modal chromosome copy number within each colony (Figures 3A and 3B). Thus, CIN cells treated with UMK57 for extended time periods maintain karyotypic heterogeneity, despite the fact that it suppresses chromosome mis-segregation in this cell line when measured immediately (Figures 2A–2D). This cellular response was not observed previously when CIN was suppressed by overexpression of MCAK or Kif2b (Bakhoum et al., 2009b), indicating a distinction between protein overexpression and chemical enhancement of protein activity as methods to suppress CIN in cancer cells.

Serial transfer of culture media over multiple days followed by immediate quantification of chromosome segregation defects in U2OS cells verifies that UMK57 retains biological activity in culture media for up to 120 hr (Figure S3A). Nevertheless, lagging chromosome rates in cells treated with UMK57 return to control levels within 72 hr (Figure 3C), and this phenomenon was also observed if media containing UMK57 was renewed every 24 hr (Figure S3B). This time-dependent decrease in responsiveness to UMK57 was also observed in multiple CIN cancer cell lines (Figures 3D–3F). In addition, verapamil, a potent inhibitor of the multidrug efflux pump encoded by the MDR1 gene, was effective at enhancing the response of these cells to doxorubicin (Figures S3C and S3D), but it did not significantly alter the decrease in responsiveness to UMK57 (Figures 3D–3F). This suggests that resistance to UMK57 occurs independently of multidrug efflux pump activity.

Aurora B Kinase Influences the Rate of Resistance to UMK57

We then focused on the events that change in mitotic cells during extended treatment with UMK57. Kinetochore-microtubule attachment stability in metaphase cells is reduced equivalently in cells treated with UMK57 for 1 hr or 72–120 hr, thus verifying the persistent UMK57-dependent MCAK activation during extended treatment (Figures 2E and 4A). Accordingly, the quantity of phosphorylated MCAK at centromeres does not change between cells treated with

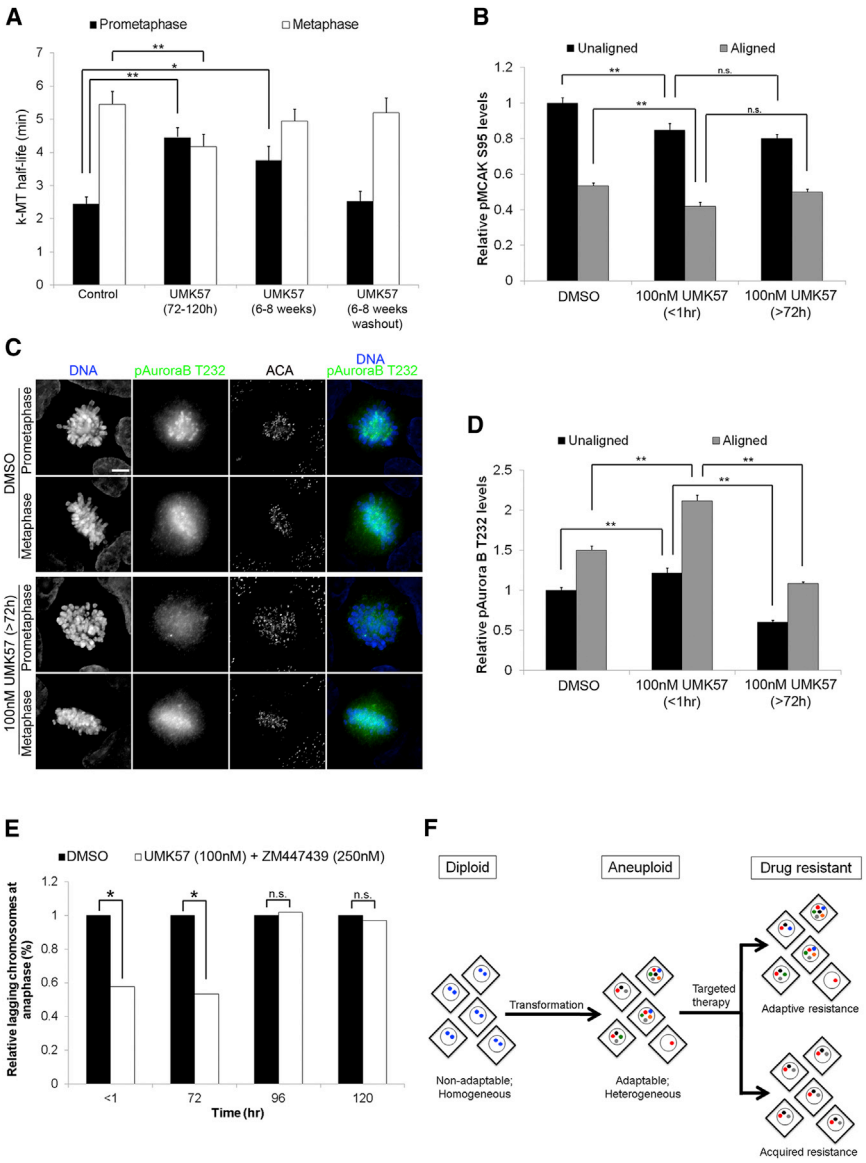

Figure 4. Rate of Adaptive Resistance in UMK57-Treated Cells Is Dependent on Aurora B Activity

(A) Calculated k-MT stability for U2OS cells treated with UMK57 for 72–120 hr or 6–8 weeks or for 6–8 weeks followed by UMK57 washout (72–120 hr post-washout). n = 10–42 cells. Graph shows mean ± SEM. Statistical analysis performed between control and UMK57-treated cells for each mitotic phase. *$p \leq 0.05$; **$p \leq 0.01$ using two-tailed t test.

(B) Quantification of the relative levels of phospho-MCAK Ser95 at kinetochores and centromeres in U2OS cells treated with UMK57 for <1 hr or >72 hr as quantified by immunofluorescence.

(C) Representative image of U2OS cells in prometaphase and metaphase treated with DMSO or UMK57 for 72 hr, fixed and stained to reveal DNA (blue), phospho-Aurora B Thr232 (green), and ACA. Scale bar, 5 μm.

(D) Quantification of phospho-Aurora B Thr232 at kinetochores and centromeres in U2OS cells treated with UMK57 for <1 hr or >72 hr as quantified by immunofluorescence. n ≥ 300 kinetochores from 10–20 cells for quantification of phospho-MCAK S95 and phospho-Aurora B Thr232. **$p \leq 0.0$; n.s., $p > 0.05$ using two-tailed t test.

(E) Media with DMSO or ZM447439 + UMK57 was prepared and added to cells at time 0. Cells were fixed and stained at <1 hr, 72 hr, 96 hr, and 120 hr and lagging chromosome rates quantified for each time point (n ≥ 150 anaphases). *$p \leq 0.05$; n.s., $p > 0.05$ using Fisher's exact two-tailed test.

(F) Conceptual model for adaptive and acquired drug resistance in CIN cancer cells. Non-transformed diploid cells are non-adaptable and genetically homogeneous. Upon oncogenic transformation, the resulting tumor cells become both adaptable to stressful conditions and karyotypically heterogeneous through chromosomal instability. Adaptive resistance arises through the rapid and reversible changes in intracellular signaling networks within the genetically heterogeneous population. Acquired drug resistance occurs through the selection of rare, genetically unique cells from the population of heterogeneous cells. These mechanisms of resistance are not mutually exclusive.

All error bars represent SEM.

UMK57 for 1 hr or >72 hr (Figure 4B), suggesting MCAK levels remain unchanged within this time frame. Moreover, extended treatment with UMK57 did not change the fractions of microtubules in the stable (k-MT) versus unstable (non-k-MT) populations or in the turnover rate of the unstable population in UMK57-treated cells (Figures S3E–S3H). In contrast, k-MT attachment stability in prometaphase cells significantly increases upon exposure to UMK57 for 72–120 hr or 6–8 weeks (Figure 4A), the latter being a time frame that mimics the clonal cell growth assay (Figures 3A and 3B). Strikingly, these changes in k-MT attachment stability in response to UMK57 treatment are reversible upon UMK57 removal (Figure 4A).

In addition to the stabilization of k-MT attachments in prometaphase, there is a substantial reduction in active Aurora B kinase at centromeres in cells treated with UMK57 for >72 hr (Figures 4C and 4D). However, this did not lead to corresponding changes in substrate phosphorylation, as phopsho-KNL1 levels were specifically increased at unaligned kinetochores (Figure S3I) and there were no changes in phospho-Hec1 levels (Figure S3J). This suggests that the Aurora B signaling network (e.g., the spatially regulated activities of both the kinase and the counteracting phosphatases) is altered in cells exposed to UMK57 for >72 hr. Thus, the capacity of UMK57 to initially improve chromosome segregation fidelity in CIN cancer cells by destabilizing k-MT attachments in metaphase is superseded

after just a few days of UMK57 treatment by changes in Aurora B kinase signaling and hyperstabilization of k-MT attachments in prometaphase. Consistently, single-cell clones grown continuously in the presence of UMK57 display reduced sensitivity to the Aurora B inhibitor ZM447439 but show no changes in sensitivity to other compounds such as doxorubicin, Taxol, vinblastine, or BI-2536 (Figures S4A–S4G).

Next, we dampened Aurora B kinase signaling using the inhibitor ZM447439 at a dose (250 nM) sufficient to partially inhibit Aurora B kinase activity as determined by the effect on phosphorylation of histone H3 at Ser10 in early prometaphase (Figure S4H). Partial inhibition of Aurora B kinase signaling does not increase lagging chromosome rates or affect the ability of UMK57 to reduce lagging chromosome rates in U2OS cells when measured within 1 hr (Figure S4I). However, partial inhibition of Aurora B kinase activity prevents cells from regaining high levels of lagging chromosomes in anaphase after treatment with UMK57 for 72 hr (Figures 4E and S4J). Partial Aurora B kinase inhibition also delayed the emergence of resistance to UMK57 in SW-620 cells (Figure S4K) but did not do so in HeLa cells (Figure S4L). This demonstrates that changes in the Aurora B kinase signaling pathway are a common means to develop resistance to UMK57 and that the full dynamic range of Aurora B kinase signaling is required for the emergence of this resistance within a 72-hr time frame. The effect of partial Aurora B kinase inhibition in preventing resistance to UMK57 was only transient, because cells ultimately regained high rates of lagging chromosomes in anaphase by 96 hr in the presence of UMK57 and the Aurora B kinase inhibitor (Figures 4E and S4K). Thus, cells achieve resistance to UMK57 through multiple pathways, suggesting that there is strong selective pressure to maintain high levels of chromosome mis-segregation in CIN cancer cells.

This work demonstrates that CIN cancer cells can systematically alter mitotic signaling pathways to generate resistance to therapies designed to target the specific mitotic defects that cause persistent chromosome mis-segregation. Emergence of resistance through rapid and reversible alterations of cellular signaling pathways is defined as adaptive resistance (Figure 4F). This is distinct from acquired resistance (Duesberg et al., 2000; Gerlinger and Swanton, 2010; Gottesman, 2002) that arises through the selection of rare, genetically unique cells from heterogeneous populations (Figure 4F). Other distinguishing features of cells that become drug resistant through an adaptive mechanism is the retention of genome complexity in the population (Figure 4F), as we observed in our FISH experiments (Figures 3A and 3B), and the emergence of resistance at sublethal doses (Figures 3D–3F and S2A). However, it is likely that both adaptive and acquired resistance contribute to drug resistance in a tumor cell population.

Adaptive resistance has been previously described in bacterial (Fernández et al., 2011) and fungal (Walker et al., 2010) systems and likely surfaces in tumor cells based on their need to tolerate the myriad stresses associated with their microenvironment and unrestrained growth (proteotoxic, mitotic, oxidative, DNA damage, and metabolic) (Luo et al., 2009). The capacity of cells to undergo adaptive resistance is rooted in cellular signaling and/or transcriptional networks that involve feedback-dependent homeostatic control (Chandarlapaty, 2012; Pisco et al., 2013), such as the mechanisms proposed to regulate k-MT attachment stability during mitosis (Godek et al., 2015). Importantly, these data suggest that the oncogenic pathways that drive cellular transformation impose changes onto the signaling networks that regulate chromosome segregation fidelity during mitosis (Orr and Compton, 2013) to promote and preserve CIN. These results provide insight into the observations that CIN cancer cells frequently display multi-drug resistance (Lee et al., 2011) and that the efficacy of targeted therapies based on molecular profiling in tumor cells (Barretina et al., 2012; Garnett et al., 2012) has been limited by rapid alterations of cellular signaling and/or transcriptional networks responsible for generating adaptive resistance (Litvin et al., 2015; Muranen et al., 2012; Sun et al., 2014).

EXPERIMENTAL PROCEDURES

Drug Treatments

UMK57 was used for all assays at 100 nM (~5-fold lower than the calculated IC_{50} in U2OS cells) since this is the lowest concentration of UMK57 that results in maximal suppression of lagging chromosomes and was used at 100–2,000 nM for cell proliferation assays only. The following drugs were also used: Monastrol (100 μM; Tocris Bioscience), MG132 (5 μM; Sigma-Aldrich), paclitaxel (Taxol) (1–100 nM; Biotang), doxorubicin (1–100 nM; Sigma-Aldrich), vinblastine (0.1-2 nM, Sigma-Aldrich), BI-2536 (2–500 nM; synthesized in-house), ZM447439 (100–3,000 nM; Tocris Bioscience), and verapamil (6 μM; Sigma-Aldrich). All controls for drug treatment were performed using 0.1% DMSO.

Photoactivation Experiments

k-MT attachment stability was measured in U2OS cells expressing α-tubulin tagged with photoactivatable GFP (plasmid provided by Alexey Khodjakov). Differential interference contrast (DIC) microscopy was used to identify mitotic cells, and fluorescent images were generated and acquired using Quorum WaveFX- X1 spinning disk confocal system (Quorum Technologies) equipped with Mosaic digital mirror for photoactivation (Andor Technology) and Hamamatsu ImageEM camera. Cells were defined as being in prometaphase or metaphase on the basis of chromosome alignment using DIC optics. Microtubules were locally activated in one half-spindle. Fluorescence images captured every 15 s for 4 min with a 100× oil-immersion 1.4 numerical aperture objective. To quantify fluorescence dissipation after photoactivation, mean pixel intensities were quantified within a rectangular area surrounding the region of highest fluorescence intensity and background subtracted using an equally sized area from the non-activated half-spindle using Quorum WaveFX software. Fluorescence intensities were normalized to the first time point after photoactivation for each cell following background subtraction and correction for photobleaching. Correction for photobleaching was calculated by normalizing to values of fluorescence loss obtained from photoactivated 100 nM Taxol-stabilized spindles where the photoactivated region did not dissipate. To measure microtubule turnover, the average intensity at each time point was fit to a double exponential curve $A1 \times \exp(k_1 \times t) + A2 \times \exp(k_2 \times t)$ using MATLAB (MathWorks), where t is time, A1 represents the less stable (non-k-MT) population, and A2 represents the more stable (k-MT) population, with decay rates of k_1 and k_2, respectively. When the equation for the double exponential curve is solved, the rate constants as well as the percentage of microtubules for the fast (non-k-MT) and slow (k-MT) processes are obtained. The turnover half-life for each process was calculated as $-\ln 2/k$ for each population of microtubules. All experiments were performed in the presence of MG132 (5 μM) to prevent mitotic exit.

Cell Transfections

Plasmid transfections were done with FuGENE 6 (Roche Diagnostics), and cells were analyzed 24 hr later by immunofluorescence. Plasmids used were GFP (pEGFP plasmid with modified multiple cloning site to incorporate AscI

and PacI sites; gift from Aaron Straight) and GFP-Kif2b and GFP-MCAK (gifts from Linda Wordeman). Short interfering RNA (siRNA) transfections were performed using Oligofectamine (Invitrogen), and cells were analyzed 48 hr later. RNA duplexes for mock siRNA (Silencer Negative Control No. 4), Kif2b (Silencer Select Pre-designed; 5′-GGACCUGGAUAUCAUCACCtt-3′), or MCAK (Silencer Select Validated siRNA; 5′-CAAAGUAUCUGGAGAACCAtt-3′) were purchased from Ambion and used at a concentration of 200 nM.

Chromosome Mis-segregation Assay

To analyze chromosome segregation in interphase cells, cells were arrested in mitosis with monastrol (100 μM) for 15 hr and then media replaced with media containing DMSO or UMK57 (100 nM). Mitotic cells were isolated by shake-off and plated at low density on coverslips for 8 hr (to allow cells to complete cytokinesis and re-enter interphase). For fixing, cells were pre-extracted with pre-warmed PHEM with 1% Triton X-100 for 5 min then fixed with 3.5% paraformaldehyde. Cells stained with DAPI and mounted using ProLong Gold antifade reagent (Molecular Probes).

CIN Assay

U2OS or RPE-1 cells plated at a low density (50–100 cells/plate) in 100-mm plates, and single-cell clones were subsequently isolated and expanded gradually until each clone occupied two 100-mm plates as a monolayer (6–8 weeks for U2OS cells; 4–6 weeks for RPE-1 cells). Cells were then rinsed with PBS, treated with KCl (75 mM) for 30 min, and fixed in and washed twice with methanol-acetic acid (3:1). FISH was performed using centromeric α-satellite probes for chromosomes 2 and 3 (Cytocell) according to manufacturer's instructions.

SUPPLEMENTAL INFORMATION

Supplemental Information includes Supplemental Experimental Procedures and four figures and can be found with this article online at http://dx.doi.org/10.1016/j.celrep.2016.10.030.

AUTHOR CONTRIBUTIONS

Conceptualization, B.O. and D.A.C.; Methodology, B.O. and D.A.C.; Formal Analysis, B.O.; Resources, L.T. and B.H.K.; Writing – Original Draft, B.O. and D.A.C.; Writing – Review & Editing, B.H.K., B.O., and D.A.C.; Visualization, B.O. and D.A.C.; Supervision, D.A.C.; Funding Acquisition, B.H.K. and D.A.C.

ACKNOWLEDGMENTS

Inquiries related to chemical compounds should be sent to B.H.K. We thank all members of our laboratory for stimulating discussions and critical feedback in the interpretation and analysis of results. We also thank Jennifer DeLuca, Iain Cheeseman, Ryoma Ohi, and Dave Cortez for kindly providing important materials and reagents. This work was supported by grant GM51542 from the National Institutes of Health (D.A.C.). B.H.K acknowledges funding support from the Canadian Institute of Health Research (MOP-97928), the Cancer Research Society (CRS; 20374), the Institute for Research in Immunology and Cancer (IRIC), and IRICoR.

Received: April 16, 2016
Revised: June 5, 2016
Accepted: October 11, 2016
Published: November 8, 2016

REFERENCES

Arrowsmith, C.H., Audia, J.E., Austin, C., Baell, J., Bennett, J., Blagg, J., Bountra, C., Brennan, P.E., Brown, P.J., Bunnage, M.E., et al. (2015). The promise and peril of chemical probes. Nat. Chem. Biol. *11*, 536–541.

Bakhoum, S.F., Genovese, G., and Compton, D.A. (2009a). Deviant kinetochore microtubule dynamics underlie chromosomal instability. Curr. Biol. *19*, 1937–1942.

Bakhoum, S.F., Thompson, S.L., Manning, A.L., and Compton, D.A. (2009b). Genome stability is ensured by temporal control of kinetochore-microtubule dynamics. Nat. Cell Biol. *11*, 27–35.

Bakhoum, S.F., Danilova, O.V., Kaur, P., Levy, N.B., and Compton, D.A. (2011). Chromosomal instability substantiates poor prognosis in patients with diffuse large B-cell lymphoma. Clin. Cancer Res. *17*, 7704–7711.

Bakhoum, S.F., Silkworth, W.T., Nardi, I.K., Nicholson, J.M., Compton, D.A., and Cimini, D. (2014). The mitotic origin of chromosomal instability. Curr. Biol. *24*, R148–R149.

Barretina, J., Caponigro, G., Stransky, N., Venkatesan, K., Margolin, A.A., Kim, S., Wilson, C.J., Lehár, J., Kryukov, G.V., Sonkin, D., et al. (2012). The Cancer Cell Line Encyclopedia enables predictive modelling of anticancer drug sensitivity. Nature *483*, 603–607.

Chandarlapaty, S. (2012). Negative feedback and adaptive resistance to the targeted therapy of cancer. Cancer Discov. *2*, 311–319.

Duesberg, P., Stindl, R., and Hehlmann, R. (2000). Explaining the high mutation rates of cancer cells to drug and multidrug resistance by chromosome reassortments that are catalyzed by aneuploidy. Proc. Natl. Acad. Sci. USA *97*, 14295–14300.

Ertych, N., Stolz, A., Stenzinger, A., Weichert, W., Kaulfuß, S., Burfeind, P., Aigner, A., Wordeman, L., and Bastians, H. (2014). Increased microtubule assembly rates influence chromosomal instability in colorectal cancer cells. Nat. Cell Biol. *16*, 779–791.

Fernández, L., Breidenstein, E.B.M., and Hancock, R.E.W. (2011). Creeping baselines and adaptive resistance to antibiotics. Drug Resist. Updat. *14*, 1–21.

Garnett, M.J., Edelman, E.J., Heidorn, S.J., Greenman, C.D., Dastur, A., Lau, K.W., Greninger, P., Thompson, I.R., Luo, X., Soares, J., et al. (2012). Systematic identification of genomic markers of drug sensitivity in cancer cells. Nature *483*, 570–575.

Geigl, J.B., Obenauf, A.C., Schwarzbraun, T., and Speicher, M.R. (2008). Defining 'chromosomal instability'. Trends Genet. *24*, 64–69.

Gerlinger, M., and Swanton, C. (2010). How Darwinian models inform therapeutic failure initiated by clonal heterogeneity in cancer medicine. Br. J. Cancer *103*, 1139–1143.

Godek, K.M., Kabeche, L., and Compton, D.A. (2015). Regulation of kinetochore–microtubule attachments through homeostatic control during mitosis. Nat. Rev. Mol. Cell Biol. *16*, 57–64.

Gottesman, M.M. (2002). Mechanisms of cancer drug resistance. Annu. Rev. Med. *53*, 615–627.

Greaves, M., and Maley, C.C. (2012). Clonal evolution in cancer. Nature *481*, 306–313.

Heppner, G.H. (1984). Tumor heterogeneity. Cancer Res. *44*, 2259–2265.

Kleyman, M., Kabeche, L., and Compton, D.A. (2014). STAG2 promotes error correction in mitosis by regulating kinetochore-microtubule attachments. J. Cell Sci. *127*, 4225–4233.

Lampson, M.A., and Kapoor, T.M. (2005). The human mitotic checkpoint protein BubR1 regulates chromosome-spindle attachments. Nat. Cell Biol. *7*, 93–98.

Lee, A.J.X., Endesfelder, D., Rowan, A.J., Walther, A., Birkbak, N.J., Futreal, P.A., Downward, J., Szallasi, Z., Tomlinson, I.P.M., Howell, M., et al. (2011). Chromosomal instability confers intrinsic multidrug resistance. Cancer Res. *71*, 1858–1870.

Lengauer, C., Kinzler, K.W., and Vogelstein, B. (1997). Genetic instability in colorectal cancers. Nature *386*, 623–627.

Litvin, O., Schwartz, S., Wan, Z., Schild, T., Rocco, M., Oh, N.L., Chen, B.-J., Goddard, N., Pratilas, C., and Pe'er, D. (2015). Interferon α/β enhances the cytotoxic response of MEK inhibition in melanoma. Mol. Cell *57*, 784–796.

Luo, J., Solimini, N.L., and Elledge, S.J. (2009). Principles of cancer therapy: oncogene and non-oncogene addiction. Cell *136*, 823–837.

Muranen, T., Selfors, L.M., Worster, D.T., Iwanicki, M.P., Song, L., Morales, F.C., Gao, S., Mills, G.B., and Brugge, J.S. (2012). Inhibition of PI3K/mTOR

leads to adaptive resistance in matrix-attached cancer cells. Cancer Cell *21*, 227–239.

Orr, B., and Compton, D.A. (2013). A double-edged sword: how oncogenes and tumor suppressor genes can contribute to chromosomal instability. Front. Oncol. *3*, 164.

Pisco, A.O., Brock, A., Zhou, J., Moor, A., Mojtahedi, M., Jackson, D., and Huang, S. (2013). Non-Darwinian dynamics in therapy-induced cancer drug resistance. Nat. Commun. *4*, 2467.

Sotillo, R., Schvartzman, J.-M., Socci, N.D., and Benezra, R. (2010). Mad2-induced chromosome instability leads to lung tumour relapse after oncogene withdrawal. Nature *464*, 436–440.

Sun, C., Wang, L., Huang, S., Heynen, G.J.J.E., Prahallad, A., Robert, C., Haanen, J., Blank, C., Wesseling, J., Willems, S.M., et al. (2014). Reversible and adaptive resistance to BRAF(V600E) inhibition in melanoma. Nature *508*, 118–122.

Talje, L., Ben El Kadhi, K., Atchia, K., Tremblay-Boudreault, T., Carreno, S., and Kwok, B.H. (2014). DHTP is an allosteric inhibitor of the kinesin-13 family of microtubule depolymerases. FEBS Lett. *588*, 2315–2320.

Thompson, S.L., and Compton, D.A. (2008). Examining the link between chromosomal instability and aneuploidy in human cells. J. Cell Biol. *180*, 665–672.

Thompson, S.L., and Compton, D.A. (2011). Chromosome missegregation in human cells arises through specific types of kinetochore-microtubule attachment errors. Proc. Natl. Acad. Sci. USA *108*, 17974–17978.

Walker, L.A., Gow, N.A.R., and Munro, C.A. (2010). Fungal echinocandin resistance. Fungal Genet. Biol. *47*, 117–126.

Zhai, Y., Kronebusch, P.J., and Borisy, G.G. (1995). Kinetochore microtubule dynamics and the metaphase-anaphase transition. J. Cell Biol. *131*, 721–734.